Electronic Supplementary Information

Selective dealloying of chemically disordered Pt-Ni bimetallic nanoparticles for the oxygen reduction reaction

Tae-Yeol Jeon,*[a] Han-Koo Lee,[a] Geon-Hee Yoon,[b] Si-Hwan Lee,[b] Hyung Joong Yun,[c] Ki-Jeong Kim,[a] Kug-Seung Lee,[a] Nicola Pinna,[d] and Seung-Ho Yu*[b]

[a]Pohang Accelerator Laboratory (PAL), Pohang University of Science and Technology, Pohang 37673, Republic of Korea

[b]Department of Chemical and Biological Engineering, Korea University, Seoul 02841, Republic of Korea

[c]Research Center for Materials Analysis, Korea Basic Science Institute (KBSI), Daejeon 34133, Republic of Korea

[d]Institute für Chemie and IRIS Adlershof, Humboldt-Universität zu Berlin, Brook-Taylor-Str. 2, 12489 Berlin, Germany

*Corresponding authors: tjeon@postech.ac.kr (T.-Y. Jeon), seunghoyu@korea.ac.kr (S.-H. Yu)

Table of Contents

Supplementary Tables

Table S1 Chemical composition from ED-XRF, peak position of (220) peak from XRD, and the resulting lattice parameter and alloying level.

Catalyst	Atomic ratio by ED-XRF (%)			XRD		
	Pt (at%)	Ni (at%)	Metal loading (wt%)[a]	2θ of (220)	Lattice parameter (Å)[b]	Alloying level (%)[c]
PR	55.8	44.2	38.1	55.070	3.793	74.9
HQ1	65.2	34.8	35.7	54.933	3.802	95.2
HQ2	65.8	34.2	35.6	54.770	3.812	89.2
HQ3	67.8	32.2	35.1	54.685	3.817	90.6
HQ4	68.8	31.2	34.9	54.630	3.821	91.5
HQ5	69.1	30.9	33.5	54.557	3.826	93.5
SA1	73.6	26.4	34.1	54.409	3.835	93.6
SA2	75.3	24.7	33.8	54.141	3.853	82.0
SA3	77.5	22.5	33.4	54.073	3.857	85.3
SA4	78.1	21.9	33.3	54.016	3.861	83.2
SA5	78.4	21.6	33.3	53.972	3.864	81.2

[a]metal loading was calculated with Pt-to-Ni ratios under the assumption of the complete reduction of Pt precursor ($PtCl_4$).

[b]lattice parameter was calculated with the peak position of (220).

[c]alloying level indicates how close to Vegard's line the lattice parameter is.

Table S2 Summary of the surface areas and activities determined by electrochemical methods.

Catalysts	Q_H[a] (mC)	$ECSA_H$[b] (m^2/g_{Pt})	$E_{1/2}$[c] (V)	i_k[d] (A/g_{Pt} at 0.9 V)
Pt/C	742	63.7	0.899	65.0
PR	292	45.0	0.883	82.8
HQ1	338	52.0	0.907	135.9
HQ2	306	47.1	0.911	146.6
HQ3	385	43.9	0.898	114.9
HQ4	263	40.5	0.893	102.0
HQ5	279	43.0	0.897	113.3
SA1	245	37.8	0.887	91.0
SA2	253	38.9	0.884	83.4
SA3	228	35.1	0.881	78.0
SA4	199	30.6	0.887	89.1
SA5	168	25.8	0.889	93.2

[a]Charge of hydrogen desorption.

[b]$Mass_{Pt}$-specific electrochemical active surface area (ECSA).

[c]Half-wave potential.

[d]$Mass_{Pt}$-specific ORR activity.

Table S3 *d*-band centers of Pt-Ni catalysts and commercial Pt/C at 140 eV and 400 eV of photon energies.

Catalysts	*d*-band center relative to Fermi level (eV)			
	hν = 140 eV		hν = 400 eV	
Pt/C	–7.63	–6.56	Pt/C	–7.63
PR	–5.69	–5.97	PR	–5.69
HQ1	–5.38	–5.26	HQ(1)	–5.38
HQ2	–6.18	–5.08	HQ(2)	–6.18
HQ3	–6.61	–4.81	HQ(3)	–6.61
HQ4	–6.54	–5.35	HQ(4)	–6.54
HQ5	–6.42	–4.77	HQ(5)	–6.42
SA1	–6.66	–5.98	SA(1)	–6.66
SA2	–6.84	–5.98	SA(2)	–6.84
SA3	–6.74	–5.35	SA(3)	–6.74
SA4	–7.11	–5.81	SA(4)	–7.11
SA5	–7.12	–5.70	SA(5)	–7.12

Supplementary Figures

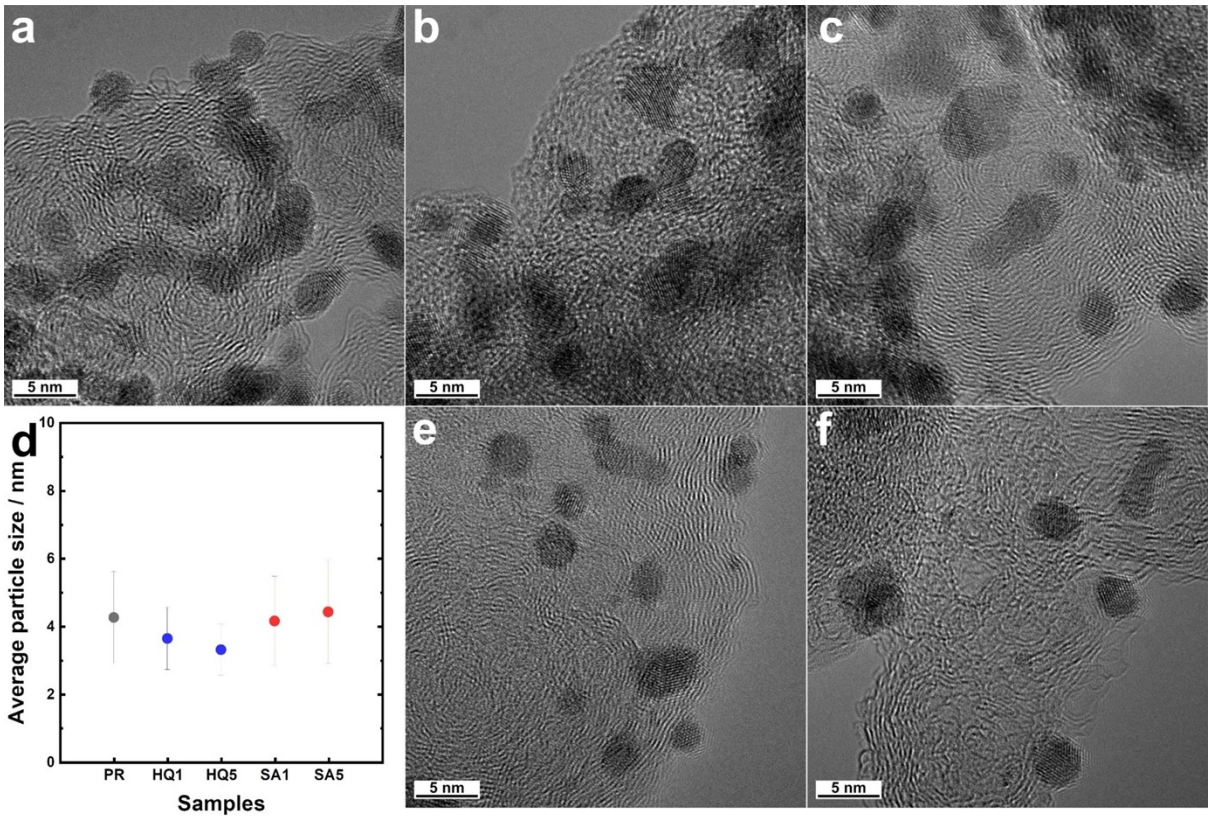

Fig. S1 TEM images and particle size distribution. Transmission electron micrograph of (a) PR, (b) HQ1, (c) HQ5, (e) SA1 and (f) SA5, and (d) their average particle diameters.

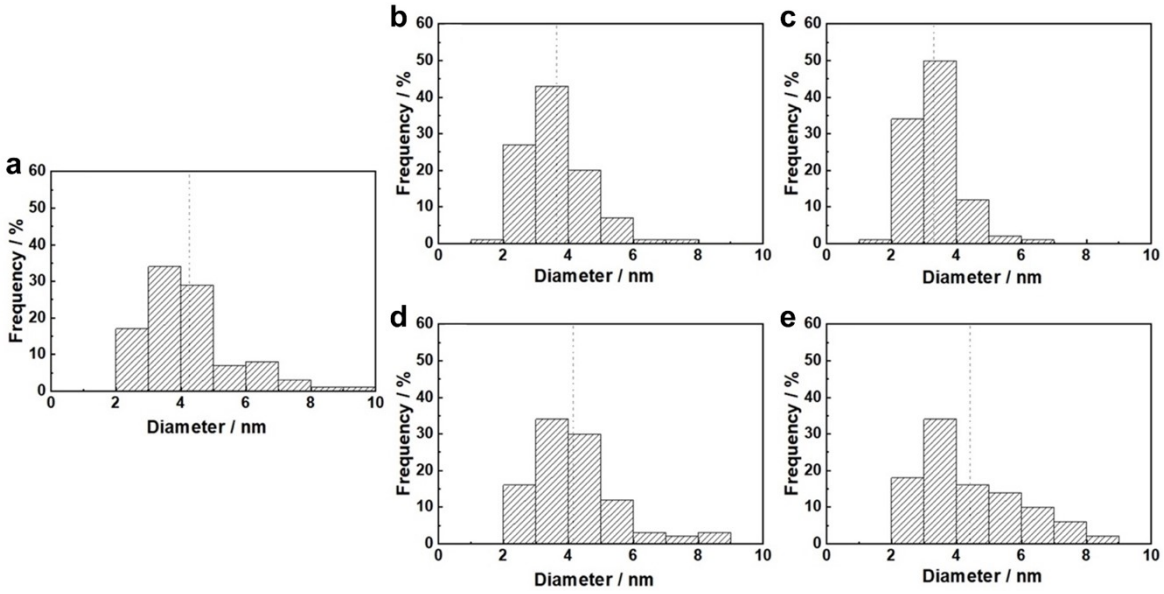

Fig. S2 Particle size distribution histograms of (a) PR, (b) HQ1, (c) HQ5, (d) SA1, and (e) SA5.

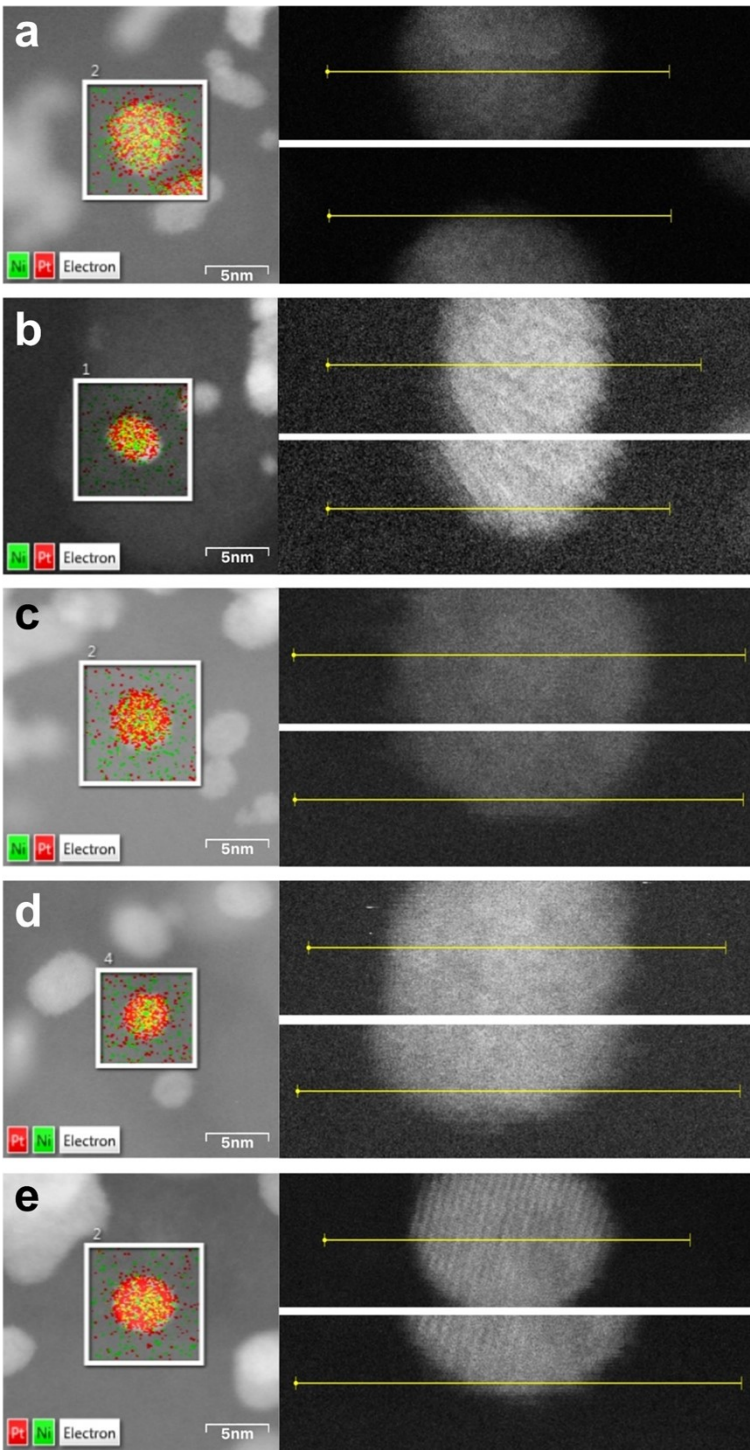

Fig. S3 TEM mapping and line scanning. High-magnification STEM image with EDS mapping of (a) PR, (b) HQ1, (c) HQ5, (d) SA1, and (e) SA5. For each catalyst, EDS line scan images are also shown on the right part and their data are plotted in **Fig. 2**.

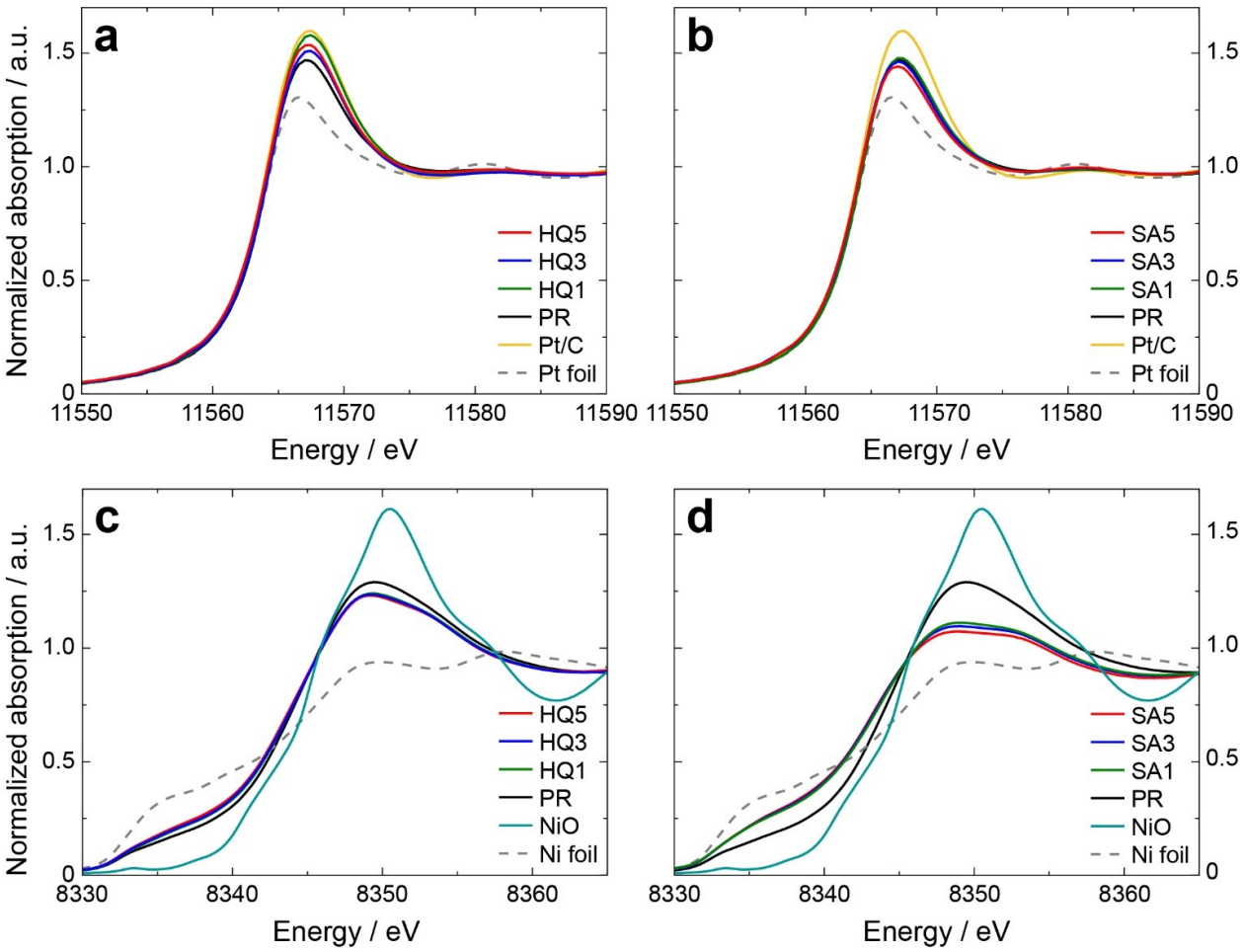

Fig. S4 X-ray absorption near edge structures of Pt L_3- and Ni K-edges. Pt L3-edge absorption spectra of (a) HQ- and (b) SA-treated Pt-Ni/C. Ni K-edge absorption spectra of (a) HQ- and (b) SA-treated Pt-Ni/C. Both NiO and Ni foil are measured to calculate the oxidation states of Ni in Pt-Ni catalysts.

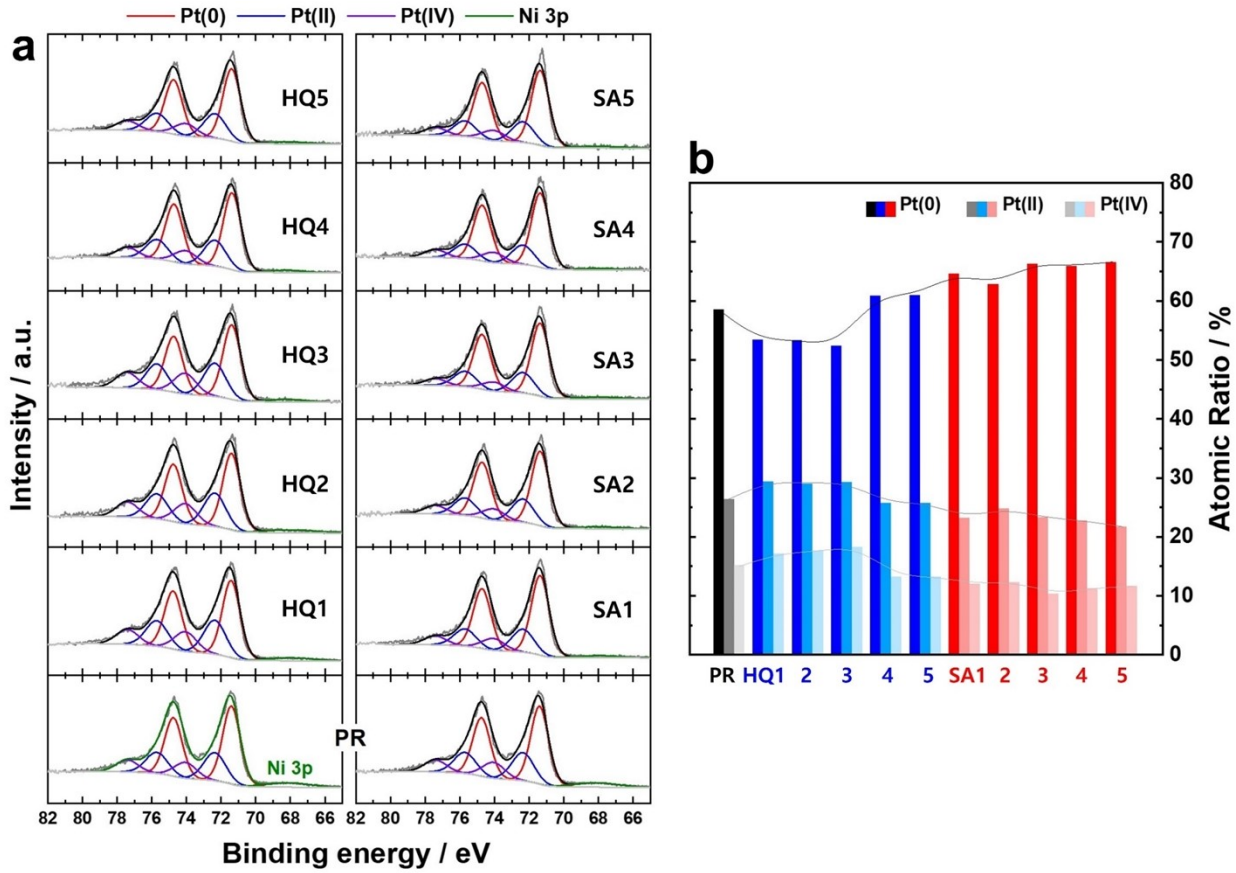

Fig. S5 Pt 4f core-level photoemission spectra. (a) Pt 4f core-level spectra of Pt-Ni catalysts measured at 140 eV of photon energy. (b) Atomic fractions of metallic Pt, Pt(II), and Pt(IV) obtained by fitting (a) the spectra. Binding energies were calibrated with respect to Au (foil) $4f_{7/2}$ at 84.1 eV. The obtained spectra were curve-fitted using CasaXPS software. Atomic ratios of different states were estimated from the areas of the respective Lorentzian-Gaussian peaks. The broad Ni 3p is also observed and included in the fitting.

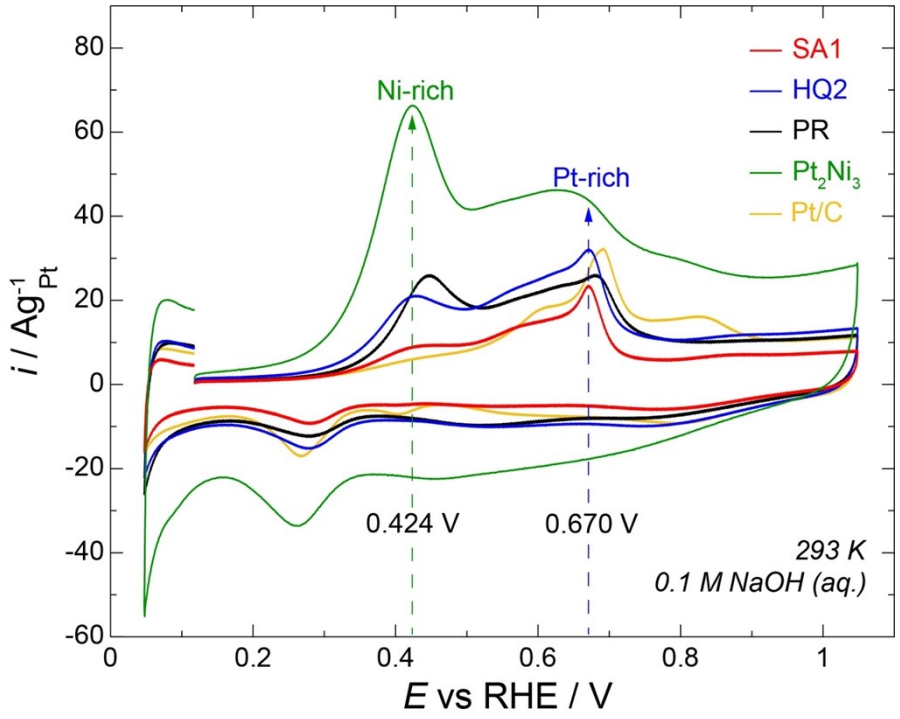

Fig. S6 CO-stripping scans for Pt-Ni and commercial Pt/C catalysts in 0.1 M NaOH (aq.). The first scan for each catalyst with a rate of 20 mV/s is plotted in the figure. Commercial Pt/C (40 wt% of Pt-loading) and Pt_2Ni_3/C (18 wt% of Pt-loading, not included in this study) are plotted as references of pure Pt and Ni-rich surfaces, respectively. Hg/HgO (0.1 M KOH, CH instruments) and glassy carbon rod were used as the reference and counter electrodes, respectively.

Discussion for Figure S6

In Fig. S6, we focused on the two main peaks associated with the oxidation of CO on specific surfaces sites at approximately 0.42 V ("prewave") and 0.67 V ("main peak"). The peaks corresponding to 0.42 V and 0.67 V are related to the prewave of high-coverage (weakly bonded) CO_{ad} and the oxidation peak of residual low-coverage (strongly bonded) CO_{ad}, respectively.[1] Typically, a Pt-rich surface has a lower prewave and a higher main peak at 0.42 V and 0.67 V, as these values are attributed to CO_{ad} on Pt atoms in proximity to oxophilic Ni oxides (NiO_x or $Ni(OH)_y$) domains and residual CO_{ad} strongly bonded to Pt atoms at higher potentials, respectively, as already reported by Strasser et al.[2]

As shown in Fig. S6, the CO-stripping voltammograms of Pt-Ni and commercial Pt/C show the order of Pt_2Ni_3>PR>HQ2>SA1>Pt/C in the prewave peak current, indicating that the surface Pt concentration of HQ2 is higher than Pt_2Ni_3 and PR, but lower than SA1 and commercial Pt/C. This result is well consistent with the STEM EDS, ED-XRD and NEXAFS results.

Supplementary Information

Info. 1 XPS Probing depths at different photon energies.

Pt 4f XPS spectra were obtained at 140 eV of the excitation photon energy at BL10A2 beamline of PAL. In the case of valence band spectra, we obtained the valence band spectra at both 400 eV and 140 eV energies. We can expect the spectra only from the few surface layers owing to the dependence of probing depth on electron kinetic energy. Probing depth is called also as inelastic electron mean free path (IMFP). The IMFP vs. electron kinetic energy (K.E.) dependency, which is called a universal curve for IMFP. According to the universal curve, the IMFPs and the probing depths are calculated as follow:

For Pt $4f_{7/2}$ at $h\nu$ = 140 eV (K.E. = 140-71 = 69 eV), IMFP = 0.48 nm, probing depth ~1.4 nm.

For valence band at $h\nu$ = 400 eV (K.E. = 400 eV), IMFP = 1.1 nm, probing depth ~3.2 nm.

For valence band at $h\nu$ = 140 eV (K.E. = 140 eV), IMFP = 0.65 nm, probing depth ~1.9 nm.

References for ESI

1. E. Herrero, Q-S. Chen, J. Hernandez, S-G. Sun, J. M. Feliu, *Phys. Chem. Chem. Phys.,* 2011, **13**, 16762-16771.
2. S. Rudi, D. Teschner, V. Beermann, W. Hetaba, L. Gan, C. Cui, M. Gliech, R. Schlogl, P. Strasser, *ACS Catal.,* 2017, **7**, 6376-6384.